Research Article | Vol. 8, No. 8 | 1 Aug 2017 | BIOMEDICAL OPTICS EXPRESS 3671
Biomedical Optics EXPRESS

Whole blood clot optical clearing for nondestructive 3D imaging and quantitative analysis

PETER HÖÖK,[1,2,9] TERESA BRITO-ROBINSON,[3,9] OLEG KIM,[1,4,5] CODY NARCISO,[3] HOLLY V. GOODSON,[6] JOHN W. WEISEL,[7,10,11] MARK S. ALBER,[1,5,8,10,12] and JEREMIAH J. ZARTMAN[3,10,13]

[1]*Department of Applied and Computational Mathematics and Statistics, University of Notre Dame, Notre Dame, IN 46556, USA*
[2]*Current address: Department of Pharmacology and Therapeutics, and Myology Institute, University of Florida, Gainesville, FL 32610, USA*
[3]*Department of Chemical and Biomolecular Engineering, University of Notre Dame, Notre Dame, IN 46556, USA*
[4]*Harper Cancer Research Institute, University of Notre Dame, IN 46617, USA*
[5]*Department of Mathematics, University of California, Riverside, CA 92521, USA*
[6]*Department of Chemistry and Biochemistry, University of Notre Dame, Notre Dame, IN 46556, USA*
[7]*Department of Cell and Developmental Biology, University of Pennsylvania School of Medicine, Philadelphia, PA 19104, USA*
[8]*Department of Medicine, Indiana University School of Medicine, Indianapolis, IN 46202, USA*
[9]*Co-first authors*
[10]*Co-corresponding authors*
[11]*weisel@mail.med.upenn.edu*
[12]*malber@nd.edu*
[13]*jzartman@nd.edu*

Abstract: A technological revolution in both light and electron microscopy imaging now allows unprecedented views of clotting, especially in animal models of hemostasis and thrombosis. However, our understanding of three-dimensional high-resolution clot structure remains incomplete since most of our recent knowledge has come from studies of relatively small clots or thrombi, due to the optical impenetrability of clots beyond a few cell layers in depth. Here, we developed an optimized optical clearing method termed cCLOT that renders large whole blood clots transparent and allows confocal imaging as deep as one millimeter inside the clot. We have tested this method by investigating the 3D structure of clots made from reconstituted pre-labeled blood components yielding new information about the effects of clot contraction on erythrocytes. Although it has been shown recently that erythrocytes are compressed to form polyhedrocytes during clot contraction, observations of this phenomenon have been impeded by the inability to easily image inside clots. As an efficient and non-destructive method, cCLOT represents a powerful research tool in studying blood clot structure and mechanisms controlling clot morphology. Additionally, cCLOT optical clearing has the potential to facilitate imaging of *ex vivo* clots and thrombi derived from healthy or pathological conditions.

OCIS codes: (170.3880) Medical and biological imaging; (170.1790) Confocal microscopy; (170.3660) Light propagation in tissues; (170.6935) Tissue characterization.

References and links

1. B. Furie and B. C. Furie, "Mechanisms of Thrombus Formation," N. Engl. J. Med. **359**(9), 938–949 (2008).
2. R. I. Litvinov, D. H. Farrell, J. W. Weisel, and J. S. Bennett, "The Platelet Integrin αIIbβ3 Differentially Interacts with Fibrin *Versus* Fibrinogen," J. Biol. Chem. **291**(15), 7858–7867 (2016).
3. M. Clarke and J. A. Spudich, "Nonmuscle contractile proteins: the role of actin and myosin in cell motility and shape determination," Annu. Rev. Biochem. **46**(1), 797–822 (1977).

#291465 https://doi.org/10.1364/BOE.8.003671
Journal © 2017 Received 30 Mar 2017; revised 12 Jun 2017; accepted 19 Jun 2017; published 17 Jul 2017

Biomedical Optics EXPRESS

4. W. A. Lam, O. Chaudhuri, A. Crow, K. D. Webster, T. D. Li, A. Kita, J. Huang, and D. A. Fletcher, "Mechanics and contraction dynamics of single platelets and implications for clot stiffening," Nat. Mater. **10**(1), 61–66 (2011).
5. R. W. Muthard and S. L. Diamond, "Blood clots are rapidly assembled hemodynamic sensors: flow arrest triggers intraluminal thrombus contraction," Arterioscler. Thromb. Vasc. Biol. **32**(12), 2938–2945 (2012).
6. W. Bergmeier and R. O. Hynes, "Extracellular matrix proteins in hemostasis and thrombosis," Cold Spring Harb. Perspect. Biol. **4**(2), a005132 (2012).
7. D. B. Cines, T. Lebedeva, C. Nagaswami, V. Hayes, W. Massefski, R. I. Litvinov, L. Rauova, T. J. Lowery, and J. W. Weisel, "Clot contraction: compression of erythrocytes into tightly packed polyhedra and redistribution of platelets and fibrin," Blood **123**(10), 1596–1603 (2014).
8. E. Pretorius, "The Role of Platelet and Fibrin Ultrastructure in Identifying Disease Patterns," Pathophysiol. Haemost. Thromb. **36**(5), 251–258 (2007).
9. T. J. Stalker, J. D. Welsh, M. Tomaiuolo, J. Wu, T. V. Colace, S. L. Diamond, and L. F. Brass, "A systems approach to hemostasis: 3. Thrombus consolidation regulates intrathrombus solute transport and local thrombin activity," Blood **124**(11), 1824–1831 (2014).
10. M. M. Kamocka, J. Mu, X. Liu, N. Chen, A. Zollman, B. Sturonas-Brown, K. Dunn, Z. Xu, D. Z. Chen, M. S. Alber, and E. D. Rosen, "Two-photon intravital imaging of thrombus development," J. Biomed. Opt. **15**(1), 016020 (2010).
11. O. V. Kim, R. I. Litvinov, J. W. Weisel, and M. S. Alber, "Structural basis for the nonlinear mechanics of fibrin networks under compression," Biomaterials **35**(25), 6739–6749 (2014).
12. N. Badiei, A. M. Sowedan, D. J. Curtis, M. R. Brown, M. J. Lawrence, A. I. Campbell, A. Sabra, P. A. Evans, J. W. Weisel, I. N. Chernysh, C. Nagaswami, P. R. Williams, and K. Hawkins, "Effects of unidirectional flow shear stresses on the formation, fractal microstructure and rigidity of incipient whole blood clots and fibrin gels," Clin. Hemorheol. Microcirc. **60**(4), 451–464 (2015).
13. A. Ertürk, K. Becker, N. Jährling, C. P. Mauch, C. D. Hojer, J. G. Egen, F. Hellal, F. Bradke, M. Sheng, and H.-U. Dodt, "Three-dimensional imaging of solvent-cleared organs using 3DISCO," Nat. Protoc. **7**(11), 1983–1995 (2012).
14. H. Hama, H. Hioki, K. Namiki, T. Hoshida, H. Kurokawa, F. Ishidate, T. Kaneko, T. Akagi, T. Saito, T. Saido, and A. Miyawaki, "ScaleS: an optical clearing palette for biological imaging," Nat. Neurosci. **18**(10), 1518–1529 (2015).
15. T. Kuwajima, A. A. Sitko, P. Bhansali, C. Jurgens, W. Guido, and C. Mason, "ClearT: a detergent- and solvent-free clearing method for neuronal and non-neuronal tissue," Development **140**(6), 1364–1368 (2013).
16. M.-T. Ke, S. Fujimoto, and T. Imai, "SeeDB: a simple and morphology-preserving optical clearing agent for neuronal circuit reconstruction," Nat. Neurosci. **16**(8), 1154–1161 (2013).
17. E. A. Susaki, K. Tainaka, D. Perrin, F. Kishino, T. Tawara, T. M. Watanabe, C. Yokoyama, H. Onoe, M. Eguchi, S. Yamaguchi, T. Abe, H. Kiyonari, Y. Shimizu, A. Miyawaki, H. Yokota, and H. R. Ueda, "Whole-Brain Imaging with Single-Cell Resolution Using Chemical Cocktails and Computational Analysis," Cell **157**(3), 726–739 (2014).
18. B. Yang, J. B. Treweek, R. P. Kulkarni, B. E. Deverman, C.-K. Chen, E. Lubeck, S. Shah, L. Cai, and V. Gradinaru, "Single-Cell Phenotyping within Transparent Intact Tissue Through Whole-Body Clearing," Cell **158**(4), 945–958 (2014).
19. E. Lee, J. Choi, Y. Jo, J. Y. Kim, Y. J. Jang, H. M. Lee, S. Y. Kim, H.-J. Lee, K. Cho, N. Jung, E. M. Hur, S. J. Jeong, C. Moon, Y. Choe, I. J. Rhyu, H. Kim, and W. Sun, "ACT-PRESTO: Rapid and consistent tissue clearing and labeling method for 3-dimensional (3D) imaging," Sci. Rep. **6**(1), 18631 (2016).
20. K. Tainaka, S. I. Kubota, T. Q. Suyama, E. A. Susaki, D. Perrin, M. Ukai-Tadenuma, H. Ukai, and H. R. Ueda, "Whole-Body Imaging with Single-Cell Resolution by Tissue Decolorization," Cell **159**(4), 911–924 (2014).
21. D. Zhu, K. V. Larin, Q. Luo, and V. V. Tuchin, "Recent progress in tissue optical clearing," Laser Photonics Rev. **7**(5), 732–757 (2013).
22. K. Tainaka, A. Kuno, S. I. Kubota, T. Murakami, and H. R. Ueda, "Chemical Principles in Tissue Clearing and Staining Protocols for Whole-Body Cell Profiling," Annu. Rev. Cell Dev. Biol. **32**(1), 713–741 (2016).
23. D. S. Richardson and J. W. Lichtman, "Clarifying tissue clearing," Cell **162**(2), 246–257 (2015).
24. J. W. Wilson, S. Degan, W. S. Warren, and M. C. Fischer, "Optical clearing of archive-compatible paraffin embedded tissue for multiphoton microscopy," Biomed. Opt. Express **3**(11), 2752–2760 (2012).
25. E. Song, H. Seo, K. Choe, Y. Hwang, J. Ahn, S. Ahn, and P. Kim, "Optical clearing based cellular-level 3D visualization of intact lymph node cortex," Biomed. Opt. Express **6**(10), 4154–4164 (2015).
26. A. F. Straight, A. Cheung, J. Limouze, I. Chen, N. J. Westwood, J. R. Sellers, and T. J. Mitchison, "Dissecting temporal and spatial control of cytokinesis with a myosin II Inhibitor," Science **299**(5613), 1743–1747 (2003).
27. J. Schindelin, I. Arganda-Carreras, E. Frise, V. Kaynig, M. Longair, T. Pietzsch, S. Preibisch, C. Rueden, S. Saalfeld, B. Schmid, J.-Y. Tinevez, D. J. White, V. Hartenstein, K. Eliceiri, P. Tomancak, and A. Cardona, "Fiji: an open-source platform for biological-image analysis," Nat. Methods **9**(7), 676–682 (2012).
28. K. Namdee, M. Carrasco-Teja, M. B. Fish, P. Charoenphol, and O. Eniola-Adefeso, "Effect of variation in hemorheology between human and animal blood on the binding efficacy of vascular-targeted carriers," Sci. Rep. **5**(1), 11631 (2015).
29. L. Silvestri, I. Costantini, L. Sacconi, and F. S. Pavone, "Clearing of fixed tissue: a review from a microscopist's perspective," J. Biomed. Opt. **21**(8), 081205 (2016).

Biomedical Optics EXPRESS

30. A. Feuchtinger, A. Walch, and M. Dobosz, "Deep tissue imaging: a review from a preclinical cancer research perspective," Histochem. Cell Biol. **146**(6), 781–806 (2016).
31. H. Hama, H. Hioki, K. Namiki, T. Hoshida, H. Kurokawa, F. Ishidate, T. Kaneko, T. Akagi, T. Saito, T. Saido, and A. Miyawaki, "ScaleS: an optical clearing palette for biological imaging," Nat. Neurosci. **18**(10), 1518–1529 (2015).
32. V. Tutwiler, R. I. Litvinov, A. P. Lozhkin, A. D. Peshkova, T. Lebedeva, F. I. Ataullakhanov, K. L. Spiller, D. B. Cines, and J. W. Weisel, "Kinetics and mechanics of clot contraction are governed by the molecular and cellular composition of the blood," Blood **127**(1), 149–159 (2016).
33. S. Zhu, B. A. Herbig, R. Li, T. V. Colace, R. W. Muthard, K. B. Neeves, and S. L. Diamond, "In microfluidico: Recreating in vivo hemodynamics using miniaturized devices," Biorheology **52**(5-6), 303–318 (2016).
34. P. M. Kulesa, J. M. Teddy, M. Smith, R. Alexander, C. H. Cooper, R. Lansford, and R. McLennan, "Multispectral fingerprinting for improved in vivo cell dynamics analysis," BMC Dev. Biol. **10**(1), 101 (2010).
35. C. Narciso, K. R. Cowdrick, V. Zellmer, T. Brito-Robinson, P. Brodskiy, D. J. Hoelzle, S. Zhang, and J. J. Zartman, "On-chip three-dimensional tissue histology for microbiopsies," Biomicrofluidics **10**(2), 021101 (2016).
36. J. Isern, S. T. Fraser, Z. He, and M. H. Baron, "The fetal liver is a niche for maturation of primitive erythroid cells," Proc. Natl. Acad. Sci. U.S.A. **105**(18), 6662–6667 (2008).
37. E. A. Susaki and H. R. Ueda, "Whole-body and Whole-Organ Clearing and Imaging Techniques with Single-Cell Resolution: Toward Organism-Level Systems Biology in Mammals," Cell Chem Biol **23**(1), 137–157 (2016).

1. Introduction

Blood clots (thrombi) form in response to vessel injury and prevent excessive bleeding [1]. The formation and mechanical properties of clots are largely determined by complex intermolecular interactions between cells and clotting proteins [2]. The contraction of clots, which requires the same actomyosin machinery involved in cell motility [3,4], is important for hemostasis to restore the flow of blood past obstructive clots [5], and for tissue regeneration [6]. Contraction of whole blood clots leads to a packed core of polyhedrocytes with much of the fibrin and platelets on the exterior [7]. Polyhedrocytes are the result of platelets pulling on fibrin during clot contraction; the erythrocytes are compressed from their normal biconcave shape to polyhedral shapes. The function of this packed structure is believed to stem bleeding in venous hemostasis but may preclude clot dissolution for certain pathologies due to low fibrinolytic enzyme permeability. Changes in the morphology of fibrin-platelet structures have also been associated with multiple pathological conditions such as heart attack, stroke, deep vein thrombosis, hemophilia, and many forms of cancer [8]. Acquiring three-dimensional (3D) structures of thick clots or thrombi is of immediate biomedical importance, as it would provide information about internal architecture of these clots or thrombi in various thrombotic and bleeding conditions.

Transmission electron microscopy and scanning electron microscopy (SEM) have been used to obtain detailed structural information from the clot surface or from thin sections of the clot interior. Intravital fluorescence microscopy [9,10] has enabled low-resolution studies of *in vivo* clot formation and light microscopy studies *ex vivo* [7,11,12] have obtained detailed structural information from near the clot surface. However, studies of whole clot structure taken from mouse models or patients with thrombotic disorders have lagged behind due to the presence of tightly-packed polyhedrocytes in the thrombus core rendering them optically inaccessible [7]. Furthermore, it has been difficult to study the redistribution of fibrin and platelets during clot contraction because of the same imaging limitations. Similar problems are also encountered when studying venous blood clots, which have a higher proportion of erythrocytes than arterial clots. Despite recent advances in understanding blood clot ultrastructure, fundamental aspects of how clot component interactions affect the composition and mechanical stability of clots and thrombi remain unclear.

Several methods for tissue decolorization and 3D imaging have been developed in recent years [13–25]. These methods have resulted in important advances for the understanding of biological structures and their arrangement within the 3D context of large tissues. For example, CUBIC utilizes aminoalcohols to target the removal of heme from erythrocytes [20]. However, CUBIC was optimized for clearing mouse organs and contains certain reagents that

Biomedical Optics EXPRESS

were determined to be counter-productive with a blood clot decolorizing process. Here, we report an optical clearing method termed cCLOT specifically tailored for whole blood clots or *ex vivo* thrombi. cCLOT quickly and efficiently renders clots transparent and enables fluorescence imaging of relevant 3D structures deep within clots. Importantly, the clot's ultrastructure is preserved with cCLOT, facilitating studies that link 3D clot structure to microstructure-based mechanistic models of blood clot formation and clotting pathologies. cCLOT permits imaging of structural components including fibrin and polyhedrocytes from intact ~1 mm-thick blood clots using two photon and confocal microscopy. Analysis of 3D images reconstructed from confocal z-stacks enables us to assess erythrocyte volumes and evaluate the fibrin network in the presence and absence of blebbistatin, a non-muscle myosin IIA inhibitor [26] that prevents clot contraction. We show that the fibrin network in the presence of blebbistatin is significantly perturbed from those in untreated clots with normal contraction. Interestingly, the volumes of erythrocytes were conserved throughout the clot thickness and were not found to vary significantly with depth, and remained the same in contracted versus non contracted clots suggesting that volume is conserved despite increased cellular density and that contraction does not require regulation of cell volumes. cCLOT was further validated on clots prepared from de-identified human blood, paving the way to detailed structural studies of human thrombi.

2. Materials and methods

2.1 Blood collection

Whole blood was obtained from CD-1 outbred mice by cardiac puncture following the Institutional Animal Care and Use Committee (IACUC) approved protocol IACUC #14-04-1740 and collected into acid citrate anticoagulant (9:1). Mouse blood was kept at room temperature and used within 3 hours of collection. Mice were housed at Freimann Life Science Center Animal Facility at the University of Notre Dame. De-identified human blood was purchased from ZenBio Inc. and was obtained by venipuncture from healthy donors and collected in ACD anticoagulant (9:1). This blood was used for proof-of-principle evaluation of cCLOT on clots derived from human blood. The commercial human blood was stored at 4 °C and was used in compliance with University of Notre Dame Institutional Review Board.

2.2 Blood reconstitution and fluorescence labeling

Blood samples were reconstituted as previously described [7] to allow specific fluorescent labeling. Briefly, reconstituted blood was made by mixing 60 µl of fresh citrated whole blood, 20 uL of an "erythrocyte fraction" (see below), 20 uL of platelet rich plasma (PRP) and 50 µg/ml final concentration of Alexa 564-labeled human fibrinogen (Invitrogen). To generate the PRP and the erythrocyte fraction, 1 mL of fresh citrated mouse blood was centrifuged at 190 x g for 10 minutes at room temperature. The PRP was saved and the buffy coat discarded. The pelleted erythrocytes were rinsed twice with 2 ml of PBS containing 0.5% BSA (Sigma), by spinning at 190 x g for 10 minutes after each rinse. The final volume of the pelleted erythrocytes was adjusted to 1 ml with PBS and this was kept as the erythrocyte fraction. To facilitate imaging of single cells, a portion (or all) of the erythrocyte fraction was labeled with 1 µM final concentration of Deep Red Cell Tracker (DRCT; Molecular Probes) for 1 hour at 37 °C. To remove excess DRCT, the labeled erythrocytes were rinsed twice with 6 ml of PBS + 0.5% BSA as above and spun at 930 x g for 10 minutes to discard supernatant. Alternatively, erythrocytes were labeled with WGA lectin-Alexa 488 conjugate (Molecular Probes) following the same procedure as described for DRCT labeling. The final lectin concentration used for labeling erythrocytes was 1 µg/ml. Reconstituted blood samples with low (2% v/v) concentration of DRCT or WGA lectin -labeled erythrocytes fraction were prepared by mixing 60 µl of whole blood with 2 µl (2%) labeled erythrocytes fraction with 18 µl non-labeled erythrocyte fraction and the other components as described above. The 2%

Biomedical Optics EXPRESS

labeled erythrocyte preparation was used for all the fluorescence microscopy studies (Figs. 3 thru Fig. 7) with the exception of the images in Fig. 4, middle panels (e, f, g, h) in which a high (20% v/v) concentration of DRCT-labeled erythrocytes fraction was used by mixing 60 µl of whole blood with 20 µl (20%) labeled erythrocytes fraction and the other components as described above. Clots derived from human blood (ZenBio) were prepared following the same procedure after blood was equilibrated to room temperature (RT). The purpose of labeling only a fraction of the total erythrocytes (2% or 20%) was to facilitate detailed imaging of individual erythrocyte shapes throughout the clot volume.

2.3 Blood clot preparation

Clots were made with reconstituted blood on 1 mm thick 12-well silicon gaskets, pressed onto a microscope glass slide treated with Sigmacote (Sigma). A volume of 25 µl of citrated reconstituted whole blood was added into each well and clotting was initiated by addition of a 1.8 µl mix of bovine thrombin (Sigma) and $CaCl_2$ at a final concentration of 1 U/ml and 20 mM, respectively. The gasket-slide set up was covered immediately by another Sigmacote treated glass slide to promote a flat top surface for the blood clot and to prevent samples from drying. The blood was then allowed to clot for 90 minutes at room temperature in the dark. Each prepared clot was then placed into a well of a 12-well plate and after a brief rinse in PBS the clots were fixed overnight in 10% buffered formalin by gentle rotation at RT.

2.4 Optical clearing optimization

A fixed blood clot was placed in each well of a 24-well plate and 1.25 ml of regular CUBIC-1 (25% w/w N,N,N',N'-tetrakis(2-hydroxypropyl)ethylenediamine (TED), 25% w/w urea, 15% w/w Triton X-100, 35% w/w water) [20] or cCLOT (see text for formulation) was added. Following a three hour clearing treatment of the clot samples at room temperature with gentle rotation, the solutions were collected, and the quantity of released heme was determined spectrophotometrically at A_{600}. The clots were imaged and fresh optical clearing solutions added. The procedure was repeated at 6 and 24 hours.

2.5 Scanning electron microscopy

PFA-fixed clots were cleared and washed with 0.1 M cacodylate buffer, fixed with 2% glutaraldehyde and 1% osmium tetroxide for one hour, respectively. Clots were then dehydrated in ethanol and critical point dried in liquid CO_2 and sputter coated with iridium. Samples were examined in a Magellan 400 field emission scanning electron microscope.

2.6 Perturbation of clot contraction with blebbistatin

Reconstituted fresh mouse blood was treated with blebbistatin before clot preparation at a final concentration of 0.05 mM or 0.3 mM. The samples were gently mixed and incubated for 40 minutes at room temperature. The blebbistatin-treated and non-treated mouse blood samples were used to make clots as described above.

2.7 Two photon and spinning disc confocal light microscopy

Stained and optically cleared blood clots were equilibrated and mounted in CUBIC-2 (50% w/w sucrose, 25% w/w urea, 10% w/w TED, 15% w/w water). Z-stack images were acquired using the two photon setting on a multiphoton laser scanning inverted microscope (Olympus FV1000) equipped with filter set (460–500, 520–560, 525–625, 650–700 nm) and a mode-locked Ti:sapphire laser (Mai Tai DeepSee 690–1040 nm, Spectra-Physics). The two photon setting was used with a 25X water objective (NA 1.0 WD 2 mm) with 4x digital magnification. We used 785 nm wavelength from the IR laser to excite the fluorophores and the emission spectra was collected using the following bandpass filters: Alexa 488 (500-550), Alexa 564 (575-625 nm) and DRCT 640 (650-700 nm). Z-stacks were acquired using the confocal settings of the multiphoton (Olympus FV1000) using a 60X oil objective (NA 1.42

Biomedical Optics EXPRESS

WD 150 µm). Imaging was also performed on a Nikon Eclipse T*i* confocal microscope (Nikon Instruments, Melville, NY) with a Yokogawa spinning disc (Andor Technology, South Windsor, CT). Image data were collected on an iXonEM + cooled CCD camera (Andor Technology, South Windsor, CT) using MetaMorph v7.7.9 software (Molecular Devices, Sunnyvale, CA) with a Nikon 60X oil lens (NA 1.49).

2.8 Quantitative analysis of fibrin heterogeneity in cleared clots

Confocal z-stacks of cCLOT treated clots were imaged on the Olympus confocal configuration described above at 60X magnification. Two sets of z-stacks were obtained for each clot - one from surface to 40 µm depth and another from 50 to 75 µm depth. Both sets were imaged at 0.1 µm intervals. Fiji was used for all cCLOT quantification [27]. A 25 µm-thick z-stack from 50 to 75 µm deep was extracted and a standard deviation projection performed to highlight dense aggregations of fibrin in the samples consistent with platelet aggregation present within the volume in a 2D plane. Prominent fibrin aggregates were segmented and counted in a 179 x 179 µm region using the Otsu auto thresholding algorithm with default parameters and the areas quantified using "Analyze Particles…." Two sets of 4 clots formed in the presence and absence of blebbistatin were analyzed.

2.9 Measurement of erythrocyte volumes

The average volume of mouse erythrocytes within optically cleared, reconstituted, whole blood clots at different depths and in the presence of blebbistatin were calculated using segmented z-stacks (n > 150 cells per population). To facilitate segmentation, a 2% (v/v) of DRCT-labeled erythrocyte fraction relative to total reconstituted blood was labeled with DRCT. For the analysis at different depths the sections were selected from a z-stack of 1 µm-step size slices spanning from the surface of the clot to 750 µm deep inside the clot. Images were obtained using an Olympus FV1000 two photon confocal microscope with 25x objective and 4x digital magnification. Likewise, the average volume of mouse erythrocytes in cleared clots of reconstituted whole blood in the presence of blebbistatin was calculated using z-stacks of segmented images for two different portions of the clot: surface to 40 µm (40 µm thick stack) and 50 to 75 µm (25 µm thick stack); in this case each z-stack was acquired with 0.1 µm steps using a 60x objective.

2.10 Statistics

All reported *p*-values are calculated from a two-tailed Student's t-test and are summarized in the text and are tabulated by figure in the supplementary spreadsheet (Data File 1).

3. Results and discussion

3.1 Developing an optimized optical clearing method for whole blood clots

Initially, we tested whether PFA fixed-whole blood clots could be optically cleared without destroying the clot's ultrastructure. We prepared clots from mouse reconstituted whole blood, fixed with 10% buffered formalin and treated them with CUBIC-1, a clearing solution that has been previously shown to extract heme and decolorize mouse tissues [20]. Treatment with CUBIC-1 for multiple days failed to completely clear the clot (Fig. 1(a)). CUBIC-1 is formulated for lipid extraction of brain tissue and contains a high concentration of Triton X-100, making CUBIC-1 highly viscous. We reasoned that by lowering the concentration of Triton X-100 from 15 wt. % to 0.2 wt. % the combined effect of greatly reduced viscosity and maintained cell membrane permeability would improve the solute exchange rate and more efficiently clear blood clots of the heme chromophore. The visible spectrum of solutions from PFA-fixed erythrocytes treated with either CUBIC-1 or TED aminoalcohol have previously been shown to overlap and correspond to heme with an absorbance peak at 600 nm [20]. Results from spectrophotometric analyses of heme release confirmed that all the modified

Biomedical Optics EXPRESS

solutions decolorized blood clots significantly faster than regular CUBIC-1, with 6.25% urea and 0.2% Triton X-100 solutions showing significant improvement over CUBIC-1 over 3 hours ($p < 0.001$) (Fig. 1(b)). Next, we investigated whether the concentration of TED affects the rate of clearance, the rationale being that the high viscosity of TED impairs the extraction kinetics of heme. It has been previously shown by Tainaka et al. [20] that a modified CUBIC1 solution containing 25 wt % urea and 15 wt % Triton X-100 in water without the aminoalcohol TED (0% TED), could not decolorize PFA-fixed blood suspensions. We found that best results were achieved at 25-35% TED (Fig. 1(c)), suggesting that any advantage from changes in solution viscosity is outweighed by the higher concentration of heme-extracting TED. For the remainder of the study, TED concentration was fixed at 25% as the reduced viscosity at this concentration gave marginally better clearing over the course of 3 hours than other concentrations tested, while still achieving significantly better heme clearance over a longer, 6 hour, treatment period than 5% TED ($p < 0.01$). It should be noted that 35% TED did give significantly better heme clearance than 25% TED over the 6 hour treatment period ($p < 0.05$), and would have also been a viable option for the final clearing solution.

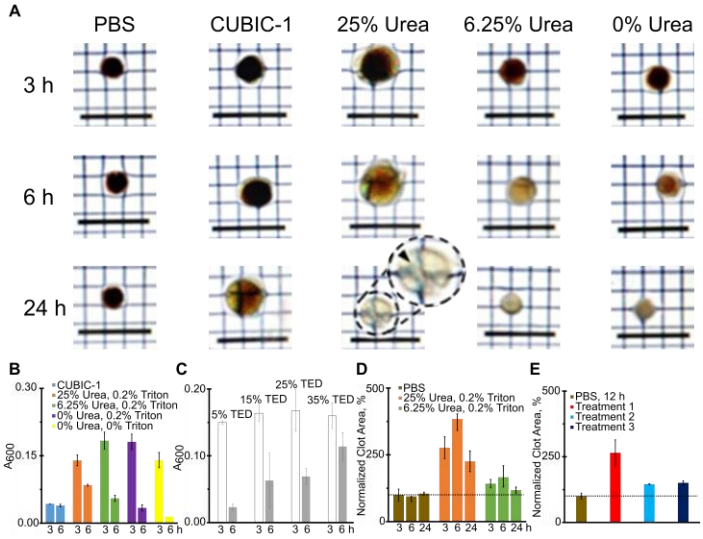

Fig. 1. Developing an optimized optical clearing method for whole blood clots. (a): Images of trans-illuminated PFA-fixed blood clots treated with PBS; CUBIC-1; or solutions containing 25% TED, 0.2% Triton X-100 and various concentrations of urea for 3, 6, and 24 h. 25% urea produced substantial clot expansion and damage. Inset in third column at 24 h: Close-up of fractured clot (arrowhead). Scale bar, 10 mm. (b): The rate of clot heme release was monitored by measuring the absorbance of clearing solutions at 600 nm following treatment at 3 hours and 6 hours with CUBIC-1 or solutions containing 25% TED and various concentrations of urea and Triton X-100. A 6.25% urea and 0.2% Triton X-100 solution significantly decolorized clots as compared to CUBIC-1 over 3 hours ($p < 0.001$) (c): Efficiency of heme release following treatment with 6.25% urea, 0.2% Triton X-100 and various concentrations of TED. Results are shown as average ± standard deviation (SD) of triplicate samples. TED of 25%-35% achieves significantly better heme clearance over a longer treatment period than 5% TED (6 h, $p < 0.01$). (d): Relative blood clot area measured at 3, 6 and 24 h. Dotted line represents 100%. A four-fold reduction in urea concentration (6.25%) produced transparent clots that were comparable in size to non-cleared control (Fig. 1(a), 1(d)) and significantly reduced the 6 h peak expansion ($p < 0.05$). (e): Excessive expansion of PFA-fixed clots following 24 hours of clearing with 6.25% urea (red, Treatment 1) could be reversed by an additional hour of treatment with PBS (light blue, Treatment 2) with a significantly reduced expansion ($p < 0.02$), followed by at least 1 hour of equilibration in CUBIC-2 (dark blue, Treatment 3). Clot area (%) for post-clearing solutions normalized to initial clot area. Dotted line represents 100%. Results reported as average ± standard deviation (SD) of triplicate samples.

Biomedical Optics EXPRESS

Urea has tissue clearing properties, but causes increased hydration and expansion of tissues [16]. To test for the effect of urea on clot clearing and morphology, clots were treated with solutions containing various concentrations of urea, while keeping the amount of TED (25%) and Triton X-100 (0.2%) constant. We found that urea contributed greatly to improving clot transparency (Fig. 1(a)). However the greater clearance at 25% urea was accompanied by significant clot expansion, with peak expansion occurring approximately 6 hours into treatment ($p < 0.01$). This drastic expansion occasionally caused the fixed clots to fracture (Fig. 1(a)). At 25% urea, clots were 2-4 times larger compared with non-cleared clots (Fig. 1(d)). A four-fold reduction in urea concentration produced transparent clots that were comparable in size to non-cleared control (Fig. 1(a), 1(d)) and significantly reduced the 6 hour peak expansion ($p < 0.05$). Equilibration of clots in PBS at room temperature for 30 min significantly reduced clearing related expansion ($p < 0.02$) in instances of substantially elevated clot size after clearing (Fig. 1(e)). Partial loss of clot transparency following PBS treatment was restored by subsequent equilibration with CUBIC-2 [20] for refractive index matching before imaging (Fig. 1(e)). This treatment did not significantly re-expand the clot after equilibration in PBS.

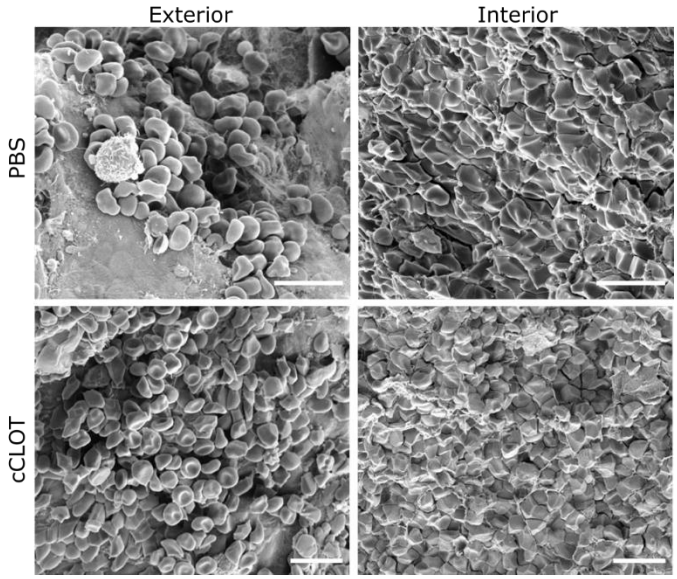

Fig. 2. Ultrastructural analysis of cCLOT-cleared blood clots. SEM images of the exterior and interior of blood clots treated with PBS or cCLOT for 24 hours. The structural arrangement with biconcave erythrocytes at the exterior and predominantly compressed polygonal-shaped erythrocytes at the interior of the clot is preserved after optical clearance. Scale bar, 10 μm.

We termed the modified and optimized CUBIC-1 derived solution: “cCLOT”, which contains 6.25% urea, 25% TED and 0.2% Triton X-100. The cCLOT protocol recommends a 30 min PBS rinse after clearing to recover the original volume of the clot, as needed. This is followed by equilibration in CUBIC-2 for at least 1 hour before imaging.

We next sought to determine whether prolonged exposure to the optimized cCLOT solution affects the intrinsic ultrastructural properties of a blood clot (Fig. 2). Blood clots were fixed and cleared as previously described and imaged by SEM. We found no visible differences in cellular morphology or overall structural arrangement between cCLOT-cleared and non-cleared blood clots (PBS), which displayed the typical packing of enclosed compressed erythrocytes in the interior and biconcave erythrocytes at the exterior [7].

Biomedical Optics EXPRESS

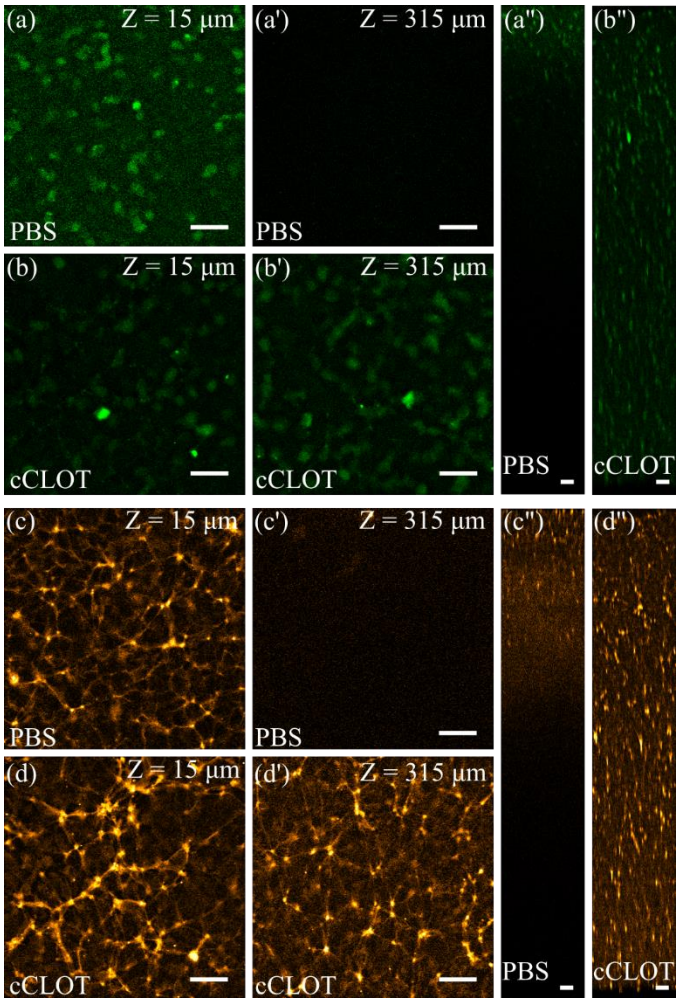

Fig. 3. PBS control vs. cCLOT-treated sample. (a, a', a" and b, b', b"): Clot erythrocytes visualized by two-photon imaging; 2% (v/v) of erythrocyte fraction relative to total reconstituted blood was stained with DRCT (Deep Red Cell Tracker). (a-a"): non-cleared control clot vs. (b-b") cCLOT-cleared clot. (a", b"): XZ orthogonal views. cCLOT enables visualization of erythrocyte shape and volume deep within the clot. (c, c', c" and d, d', d"): Clots stained for fibrin showing difference between non-cleared and cCLOT cleared clots. Note the extensive fibrin network at the outer edge and within the clot core (c", d"): XZ orthogonal views of non-cleared vs. cCLOT-cleared clots demonstrate the ability of the cCLOT method to image fibrin networks throughout the clot and at depths that exceeds control clots by ~5-fold. Entire region depicted in a", b", c" and d" represents a depth of 739 µm. Fibrin aggregates can be seen as small, closely packed irregular structures from which fibrin fibers project. Imaged with 25x water objective (1.0 NA, 4x digital magnification) with 1 µm step z-slices. Scale bars are 25 µm.

Biomedical Optics EXPRESS

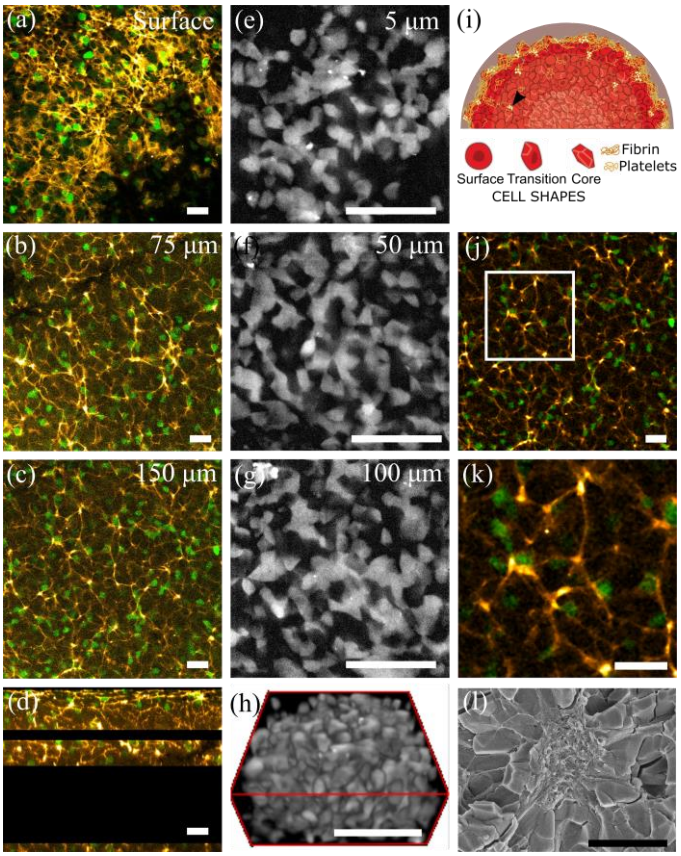

Fig. 4. Confocal microscopy of optically cleared clots. Left panels: Composite confocal images from a cCLOT-cleared clot in which fibrin is labeled with Alexa 564 fibrinogen (orange hot) and containing a 2% (v/v) of DRCT-labeled erythrocyte fraction relative to total reconstituted blood (green), (a): Clot surface, (b): 75 µm depth, (c): 150 µm depth, and (d): Orthogonal YZ view showing the Z-stacks obtained at 3 different depths of the clot. Gaps between Z-stacks were not imaged as a compromise to deal with the limited confocal scanning speed. Scale bars are 20 µm. Middle panels: Clots made with 20% (v/v) DRCT-labeled erythrocyte fraction relative to total reconstituted blood (grey) were imaged using a spinning disc confocal microscope with 60X objective lens: (e): 5 µm depth, (f): 50 µm depth, (g): 100 µm depth, and (h): 3D reconstruction of a 50 µm thick Z stack (0.1 µm steps). Scale bar, 50 µm. Panels e-h were imaged from a cCLOT solution containing 25% urea. Right panels: (i): Illustration of a blood clot with a platelet aggregate (black arrow) located deep in the clot. (j): cCLOT allows detection of red blood cells and fibrin aggregates deep within the clot (150 µm depth shown) erythrocytes and fibrin labeled as described in left panels (k): Inset from j, white square, showing magnified fibrin aggregate. (l) SEM of the exposed interior of a clot visualizing a platelet aggregate in the center of compressed erythrocytes. Note that associated fibrin fibers are not clearly visible. Scale bar, 10 µm.

3.2 cCLOT reveals the inner structure of contracted whole blood clots

As a first demonstration of the utility of the cCLOT method, two photon microscopy was performed to image 1 mm-thick optically cleared clots derived from mouse blood made with a fraction of DRCT labeled erythrocytes and Alexa 564-labeled human fibrinogen for fibrin visualization (Fig. 3, Visualization 1). Optical microscopy of non-cleared whole blood clots becomes impossible beyond a thickness of less than 20 µm, failing to reveal important details in fibrin architecture. In contrast, both the erythrocytes and fibrin network of cCLOT-treated clots could be imaged through the entire thickness of the contracted clot (>700 µm) (Fig. 3(a)" vs. Fig. 3(b)" and Fig. 3(c)" vs. Fig. 3(d)").

Biomedical Optics EXPRESS

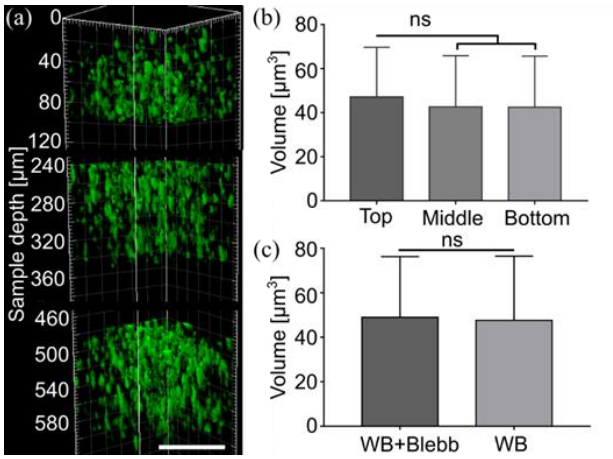

Fig. 5. Erythrocyte volumes in a contracted, cCLOT-cleared, clot at different depths (a): 3D view of clot showing sections used for erythrocyte volume calculations. Scale bar, 100 µm (b): Average volume of erythrocytes as a function of clot depth. The erythrocyte volume was measured from segmented images of z-stacks obtained at 1 µm steps in clots containing 2% v/v of DRCT-labeled erythrocyte fraction relative to total reconstituted blood (erythrocytes shown in green). Images for (a) and (b) were obtained using two photon microscopy with 25X water lens 4x digital magnification. Erythrocyte volumes in contracted versus non-contracted cCLOT cleared clots (c): Average volume of erythrocytes was measured for control non-treated reconstituted whole blood (WB) clots and clots made with blebbistatin treated reconstituted whole blood. The erythrocyte volume for (c) was measured from segmented images of z-stacks of clots containing 2% v/v of DRCT-labeled erythrocyte fraction relative to total reconstituted blood. Data for figure (c) extracted from images obtained using an Olympus confocal microscope with 60X oil lens. Z-stacks obtained at 0.1 µm steps.

Next, we imaged clots at higher magnification. Confocal microscopy is limited in imaging speed and generates large data sets, which quickly become prohibitive when the goal is to image large samples at high magnification and high resolution. We thus elected to image multiple clot samples at selected intervals through the depth of the clots. Figure 4 shows high resolution imaging of a cCLOT-cleared clot with confocal imaging using a 60x objective. The images demonstrate that cCLOT enables composite views of the fibrin network and erythrocytes in clots from whole blood at greater depths and resolution than previously possible [7]. The composite images were obtained from clots containing different fractions of erythrocytes labeled with DRCT to facilitate imaging (Fig. 4). The middle panels of Fig. 4 show erythrocytes with angular polyhedral shapes within the cleared clot (Fig. 4(e), 4(f), 4(g) and 4(h)). This result validates and extends previous findings of polyhedral compacted erythrocytes [7] in the clot interior as imaged with light microscopy and SEM. We also observe a higher density of fibrin known to be associated with platelet aggregates towards the surface of the clot (~25 µm depth within the clot's cap) (Fig. 4(a)-4(d)). Localized regions of fibrin aggregates at different depths in the clots are consistent with platelet aggregation (punctae in Fig. 4(j), 4(k)). SEM images cannot show the extent of the 3D fibrin network towards the interior of clots (Fig. 2 and Fig. 4(i), 4(l)). The extensive fibrin network with platelet aggregates very deep in the clots is consistent with the clots being formed under conditions that do not allow full contraction. Areas of compacted erythrocytes radiating from platelet aggregates as observed in the SEM (exposed core region illustrated in Fig. 4(i) and shown on Fig. 4(l)) resemble zones of the clot core architecture revealed by light microscopy (Fig. 4(j), 4(k), deep in the clot).

3.3 Quantitative analysis of erythrocyte volumes

To demonstrate the unique feasibility of the cCLOT method in providing quantitative three-dimensional cellular analysis of a clot, we measured the average volume of segmented mouse

Biomedical Optics EXPRESS

erythrocytes in a cleared clot at different depths. We found that the volume of mouse erythrocytes is conserved across different depths of the contracted clot (Fig. 5) with an average value of 44 μm^3, close to the reported mean corpuscular volume of ~40 μm^3 of mouse erythrocytes [28]. The conserved volume of erythrocytes indicates that compression as a result of clot depths does not result in fluid loss from these cells.

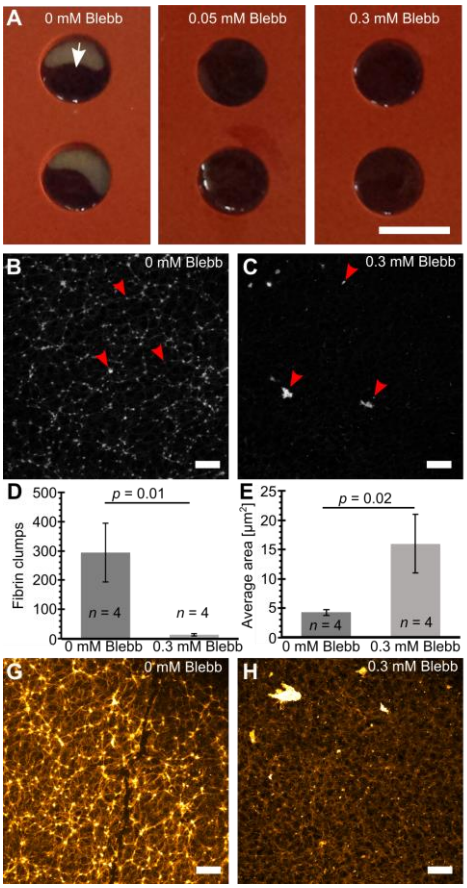

Fig. 6. Structural analysis of perturbed clots. Effects of the actomyosin inhibitor blebbistatin (Blebb) on blood clot contraction and fibrin network: (a): Normal clots contracted in the absence of blebbistatin (left, white arrow), versus non-contracted clots (right panels) made with blood pre-treated with blebbistatin (0.3 mM or 0.05 mM). Clots were made in cylindrical well chambers (5 mm diameter x 1 mm depth) on silicon gasket slides, which represent the geometry of cylindrical cross-sections. (b, c): Standard deviation projections of confocal z-stacks from contracted clots, (b), and clots where contraction was inhibited by 0.3 mM blebbistatin (c). Dramatic differences in fibrin aggregate distribution and architecture are apparent (red arrows). Projections represent a 25 μm slab sampled from ~15 μm under the clot surface and imaged on Olympus confocal configuration using 60x oil objective (d, e): Quantification of the number and size of fibrin aggregates in standard deviation projections of 25 μm slabs from 4 clots incubated with and without 0.3 mM blebbistatin. Contracted, control, clots show a significant difference in the number and size of fibrin aggregates indicative of a homogenously distributed fibrin network. Image (d) shows the average number of fibrin aggregates ± SD per region for 4 samples. Aggregates were differentiated from fibrin fibers. Image (e) shows the average area of fibrin aggregates ± SD per region for 4 samples. Quantified region at 60x represents an area of 179 x 179 μm. (g, h): Maximum intensity z-projection of a 25 μm slab (50 μm to 75 μm depth) of a contracted clot (g) and uncontracted clot formed in the presence of blebbistatin (h). Scale bars are 10 μm. Fibrin (orange hot) was imaged by incorporating Alexa 564-labeled human fibrinogen in reconstituted blood and contained 2% v/v of DRCT-labeled erythrocyte fraction relative to total reconstituted blood (erythrocytes not shown).

Biomedical Optics EXPRESS

3.4 Structural analysis of perturbed clots

In a proof-of-principle study, we tested the ability of cCLOT to reveal abnormalities in blood clot structure that were perturbed pharmacologically. Adding blebbistatin, a cell permeable specific inhibitor of non-muscle myosin II and of platelet contraction, perturbed the formation of contracted clots made with fresh mouse blood. Initial visual observation confirmed complete contraction of un-treated control clots (~30% volume reduction) whereas mouse blood treated with either 0.05 mM or 0.3 mM blebbistatin produced clots that did not contract (no volume change observed) (Fig. 6(a), 0, 0.3 and 0.05 mM blebbistatin). Following clearing with cCLOT, confocal imaging revealed qualitative changes in the appearance of the fibrin network between contracted control clots and non-contracted clots incubated with 0.3 mM blebbistatin (Fig. 6(b)-6(c)). Blebbistatin-mediated platelet actomyosin inhibition resulted in significantly fewer fibrin aggregates that differed significantly in size. These changes were quantified using Fiji as described in Methods and are shown (Fig. 6(d), 6(e)). Uncontracted clots produced with blebbistatin-treated fresh mouse blood show significantly fewer and larger fibrin aggregates than contracted control clots (Fig. 6(d)). In addition, the fibrin aggregates produced in the contracted clots exhibited more uniformly, but smaller distributed fibrin aggregates that are interconnected by fibrin fibers (Fig. 6(g)). While platelets were not stained separately, these fibrin aggregates are consistent with platelet aggregation. In contrast, uncontracted clots treated with blebbistatin lead to a non-uniform distribution of aggregated platelets corresponding to large fibrin aggregates. The fibrin network shows reduced interconnectivity, which is disrupted due to inhibition of platelet contraction (Fig. 6(h)). Importantly, cCLOT enables analysis of red blood cells throughout the clot. To test whether clot contraction results in volume compression of erythrocytes, we measured erythrocyte volumes with respect to clot depth in non-contracted and contracted clots made with the fresh mouse blood. We found that there were no significant differences between the volumes of erythrocytes in contracted clot vs. perturbed blebbistatin-treated clot (Fig. 5(c)). These results are consistent with increased clot density of contracted clots and indicate that compression as a result of clot contraction does not result in fluid loss from these cells. This analysis serves to demonstrate the quantitative utility of the cCLOT system for fully defining the structure of whole blood clots under both physiological and pathological conditions.

3.5 Application of cCLOT method to human blood

To further validate our clot-optical clearing method, we prepared thick clots with commercial de-identified human whole blood for initial evaluation studies (Fig. 7). We show the ability of imaging the complete fibrin network spanning from the clot surface to ~800 µm depth using two photon microscopy (Fig. 7(a)-7(c), Visualization 2). Additionally we were able to validate the different erythrocyte shapes at the surface of the clot (biconcave) versus deep in the clot (polyhedral) (Fig. 7(f)-7(h)). These results suggest that cCLOT will be an effective method in future studies using freshly drawn human blood or fixed samples of human thrombi.

Biomedical Optics EXPRESS

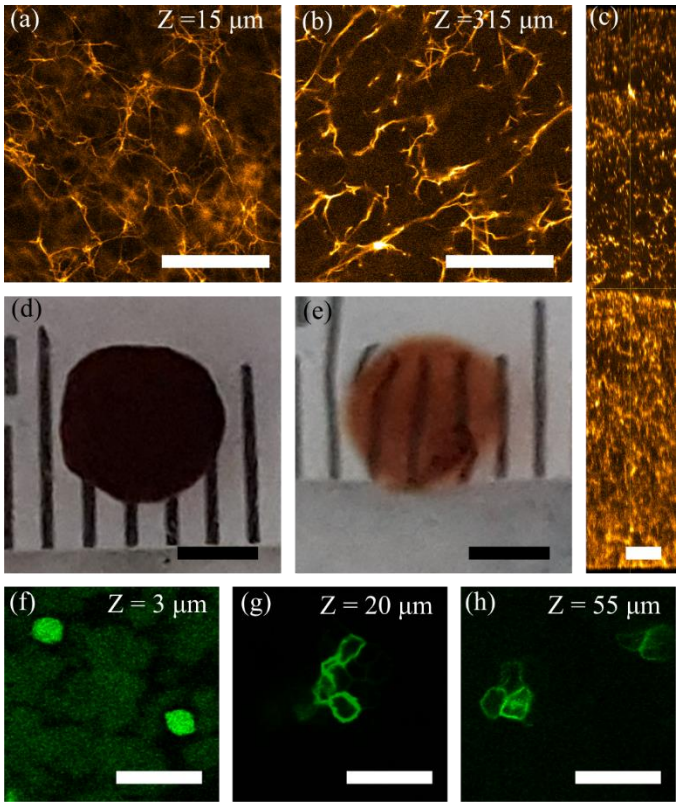

Fig. 7. cCLOT optically clears human blood clots. (a, b): Confocal microscopy z-slices of a 3D fibrin network imaged at (a) 15 µm depth and (b) 315 µm depth. (c) XZ orthogonal view of the fibrin network inside the blood clot imaged with confocal microscopy. The entire clot depth imaged is 801 µm. Fibrin (orange hot) visualized by adding Alexa 564-labeled human fibrinogen into reconstituted blood. Scale bars in (a), (b) and (c) are 50 µm. (d, e): A human blood clot before (d) and after cCLOT clearing (e). Scale bars for (d) and (e) are 2 mm. (f-h) erythrocytes imaged at different depths within the clot. Clots containing 2% (v/v) of Alexa-488 WGA lectin labeled erythrocyte fraction relative to total reconstituted volume of blood. Note erythrocytes shape changes from biconcave cells near the clot surface (f) to polyhedrocytes located in the clot interior (h). Scale bars for (f), (g), and (h) are 25 µm. All confocal images were obtained with a 60X magnification objective.

Significant progress has been made in recent years towards developing clearing solutions and protocols to facilitate fluorescence microscopy deeper into tissues [22,23,29,30]. An effort to clear whole mouse body tissues resulted in the development of CUBIC-1, which eluted heme from PFA fixed blood suspensions compatible with fluorescent protein imaging. However, we found that CUBIC-1, which efficiently clears lipid-rich mouse brain, was not able to efficiently clear PFA-fixed whole blood clots. Here, we have established and validated a modified aqueous-based clearing solution, compatible with confocal microscopy, that produces transparent blood clots at physiologically relevant millimeter size scale in less than 24 hours. cCLOT treatment enabled deep 3D fluorescence imaging while maintaining ultrastructural integrity and cellular morphology.

To the best of our knowledge, this is the first report of an optical clearing technique for a whole blood clot with the purpose of detailed visualization of its cellular and fibrous components using fluorescent confocal microscopy. Comparison of different clearing solutions and their ability to preserve synaptic structural integrity using TEM has previously shown that Sca*l*eS [31], which has a low Triton X-100 concentration (<0.2%), is best in preserving cellular membrane structure. By varying the concentrations of the clearing solution

Biomedical Optics EXPRESS

components, we found that using a low Triton X-100 concentration (cCLOT contains 0.2%) in addition to a 6.25% urea concentration (as opposed to 25% in CUBIC-1) preserves the morphology of erythrocytes, therefore overcoming problems associated with the implementation of CUBIC-1 for optical clearing of blood clots.

To demonstrate the utility of the cCLOT, we showed that reconstituted contracted whole blood clots can be imaged using two photon fluorescence microscopy to depths on the millimeter scale, whereas previous *in vitro* contracted blood clot imaging was limited to the clot surface (~20 µm deep) due to the opacity of erythrocytes. Previous findings indicated the presence of surface fibrin as well as formation of polyhedrocytes deeper in contracted clots. However, these studies were done using either SEM of clot fragments or confocal microscopy of the superficial layers (≤ 20 µm deep) [7]. Our approach provides a new solution for 3D structural visualization allowing assessment of fibrin organization and the spatial packing of erythrocytes throughout contracted clots. Additionally, we are able to visualize the structure of polyhedrocytes within the clot volume. Our results show significant impairment of clot contraction in the presence of blebbistatin, confirming previous findings indicating an important role for actomyosin in platelet-driven clot contraction [32].

Here we additionally validate the ability to optically clear opaque ~5 mm diameter x 1 mm thick clots made from pre-labeled reconstituted human blood. The cCLOT method revealed the complete fibrin network spanning the fibrin cap at the clot surface and along the inner clot. cCLOT also allowed a detailed imaging of the deformed polygonal shapes that erythrocytes under the fibrin cap (~20 um) and deeper in the clot interior as opposed to the disc-shaped erythrocytes observed at the surface.

cCLOT combined with the blood reconstitution and pre-labeling strategy presented here can be a valuable tool in basic and preclinical research for evaluating how changes in precise clot composition made from normal or drug treated blood affect clot formation, morphology and stability. Additionally, the use of microfluidic devices for studying clot formation under flow that mimics in vivo conditions as described in [33] could now be combined with pre-labeled blood components followed by fixing and cCLOT optical clearing steps, easily automated, to facilitate high resolution imaging of resulting clot composition. Such cell labeling strategies are frequently used to develop important insights into complex biological processes [34]. Also, microfluidic devices for high-throughput screening could potentially facilitate these and similar studies, and assisting in drug development [35]. Whole blood clots isolated from transgenic mice expressing selected fluorescently labeled hematopoietic markers as previously described [36] would represent an ideal type of model system to study roles of different blood cells in clot formation which could be combined with induced in vivo pathological conditions. Little is known about the structure and composition of opaque venous thrombi and how it relates to the clinical history of the patient. A very exciting application of cCLOT would be to optically clear millimeter scale *ex vivo* clots aspirated from patients. The specific labeling of cellular components will require improvements in the delivery systems of antibodies in combination with the use of smaller fluorescently labeled molecular probes including nanobodies [37].

4. Conclusions

Whole blood clots have been a challenge to image with light microscopy due to the opacity of erythrocytes. In this work, we optimized a water based optical clearing solution that renders millimeter-scale whole mouse or human blood clots transparent, while conserving the clot ultrastructure. The clearing ability was demonstrated by imaging fluorescently labeled erythrocytes and fibrin across the whole clot depth using confocal and two photon microscopy. This new method allowed the validation of the erythrocytes deformed shapes (polyhedrocytes) within the clot using confocal microscopy, as well as revealing the entire fibrin network and its interaction with the erythrocytes. This technique allows quantitative analysis of clot composition at the cellular level. We found that erythrocyte volumes do not

Biomedical Optics EXPRESS

significantly change upon clot contraction and remain the same at different depths. This supports the idea that clot contraction is achieved by increased packing efficiency of erythrocytes and not through cell volume reduction. Furthermore, we demonstrated the potential use of cCLOT in assessing drug-associated changes in fibrin organization and clot structure by evaluating fibrin aggregates in the presence of a non-muscle myosin II inhibitor drug, blebbistatin.

Funding

National Institutes of Health (NIH) (UO1 HL116330); National Science Foundation (NSF) (CBET-1403887, DMS-1517293, DMR1505662); AD&T Berry Fellowship; AD&T Discovery Awards; Harper Cancer Research Institute's Research Like a Champion award I and II; and Walther Cancer Foundation.

Acknowledgments

Imaging was supported by the Notre Dame Integrated Imaging Facility (NDIIF) and IUSM-SB Imaging Core Facility. The authors thank Nicholas Contento for comments on earlier versions of the manuscript.

Conflict of interest disclosure

The authors declare that there are no conflicts of interest related to this article.